

Table 2. Distribution of alkanes over the various channels [zigzag (z-z), straight (str.), and inter-section (int.)] of silicalite at 298 K.

n_C	z-z	str.	int.
C ₄	0.50	0.42	0.08
C ₅	0.49	0.44	0.07
C ₆	0.45	0.49	0.06
C ₇	0.41	0.54	0.05
C ₈	0.36	0.59	0.05
C ₉	0.31	0.65	0.04
C ₁₀	0.18	0.78	0.03
C ₁₁	0.18	0.79	0.04
C ₁₂	0.20	0.77	0.03

more "unidimensional" with increasing length of the hydrocarbon. Because the energetics of hydrocarbon adsorption in the two types of channels are different, this preferential adsorption influences the heats of adsorption and causes the change in slope of the heats of adsorption as a function of carbon number (see Fig. 2).

Many practical applications require knowledge of the adsorption isotherm, which gives the number of molecules adsorbed in a zeolite. Simulations of these adsorption isotherms can be performed in the grand canonical ensemble, which allows for the exchange of molecules between the zeolite and reservoir. Such simulations have been performed for small molecules (17), and use of the configurational-bias Monte Carlo technique would make it possible to simulate the adsorption isotherms of long chain alkanes under realistic conditions.

The calculation of the heat of adsorption of decane took approximately 20 hours on a workstation (18). A comparable molecular dynamics simulation would require thousands of years of supercomputer time. The saving in time is due to the fact that with the configurational-bias technique we can take advantage of special Monte Carlo moves that are impossible in nature but very efficient on a computer. In this respect it is interesting that experimentally the equilibration of decane in silicalite took 2 weeks (19). The price we had to pay for being able to perform these simulations is that we could not get direct information on the dynamics of the guest molecules. However, our method can provide the free energy of an alkane molecule as a function of its position along the channel. This free energy corrugation can subsequently be used in conjunction with transition state theory to investigate diffusion. This would be a very interesting direction for future work.

REFERENCES AND NOTES

1. Sir J. M. Thomas, *Sci. Am.* **266**, 112 (April 1992).
2. C. R. A. Catlow, Ed., *Modelling of Structure and Reactivity in Zeolites* (Academic Press, London, 1992).

3. R. L. June, A. T. Bell, D. N. Theodorou, *J. Phys. Chem.* **96**, 1051 (1992).
4. J. I. Siepmann and D. Frenkel, *Mol. Phys.* **75**, 59 (1992).
5. D. Frenkel, G. C. A. M. Mooij, B. Smit, *J. Phys. Condens. Matter* **4**, 3053 (1992).
6. J. Harris and S. A. Rice, *J. Chem. Phys.* **88**, 1298 (1988).
7. J. J. de Pablo, M. Laso, U. W. Suter, *ibid.* **96**, 6157 (1992).
8. J. I. Siepmann, S. Karaborni, B. Smit, *Nature* **365**, 330 (1993).
9. A. G. Bezus, A. V. Kiselev, A. A. Lopatkin, P. Q. Du, *J. Chem. Soc. Faraday Trans. 2* **74**, 367 (1978).
10. M. M. Dubinin, G. U. Rakhmatkariev, A. A. Isirikyan, *Izv. Akad. Nauk SSSR Ser. Khim.* **10**, 2333 (1989).
11. P. A. Jacobs, H. K. Beyer, J. Valyon, *Zeolites* **1**, 161 (1981).
12. J. Caro *et al.*, *J. Chem. Soc. Faraday Trans. 1* **81**, 2541 (1985).
13. R. E. Richards and L. V. C. Rees, *Langmuir* **3**, 335 (1987).
14. H. Thamm, *Zeolites* **7**, 341 (1987).
15. J. O. Titiloye, S. C. Parker, F. S. Stone, C. R. A. Catlow, *J. Phys. Chem.* **95**, 4038 (1991).
16. J. B. Nicholas *et al.*, *ibid.* **97**, 4149 (1993).
17. G. B. Wood, A. Z. Panagiotopoulos, J. S. Rowlinson, *Mol. Phys.* **63**, 49 (1988).
18. The simulations have been performed on an IBM RS/6000-370 workstation.
19. H. Stach, H. Thamm, K. Fiedler, W. Schirmer, in *New Developments in Zeolite Science and Technology*, Proceedings of the 6th International Zeolite Conference, D. Olsen and A. Bisio, Eds. (Butterworth, Guildford, UK, 1984), pp. 225-231.
20. J. R. Hufton and R. P. Danner, *AIChE J.* **39**, 954 (1993).
21. H. B. Abdul-Rehman, M. A. Hasanain, K. F. Loughlin, *Indian Eng. Chem. Res.* **29**, 1525 (1990).
22. H. Stach, U. Lohse, H. Thamm, W. Schirmer, *Zeolites* **6**, 74 (1986).
23. We thank M. C. Zonneville for her contribution to this work.

21 January 1994; accepted 6 April 1994

Estimates of Diapycnal Mixing in the Abyssal Ocean

John M. Toole,* Kurt L. Polzin, Raymond W. Schmitt

Profiles of diapycnal eddy diffusivity to a maximum depth of 4000 meters were derived from ocean velocity and temperature microstructure data obtained in conjunction with separate experiments in the Northeast Pacific and Northeast Atlantic oceans. These profiles indicate that in the ocean interior where the internal wave field is at background intensity, the diapycnal eddy diffusivity is small (on the order of 0.1×10^{-4} meters squared per second) and independent of depth, in apparent contradiction with large-scale budget studies. Enhanced dissipation is observed in regions of elevated internal wave energy, particularly near steeply sloping boundaries (where the eddy diffusivity estimates exceed 1×10^{-4} meters squared per second). These results suggest that basin-averaged mixing rates may be dominated by processes occurring near the ocean boundaries.

Diapycnal flow in the ocean interior, with its attendant turbulent mixing, represents the return limb of the ocean thermohaline circulation. Surface waters advected into regions of atmospheric cooling at high latitudes lose buoyancy and sink to abyssal depths and in turn displace lighter waters upward. Maintenance of the thermocline in the face of this upward advection of cold water is believed to be accomplished by downward (more precisely, diapycnal) diffusion of heat (1, 2). The intensity of the meridional overturning circulation and the diapycnal mixing in the abyss, as well as the mechanisms responsible for the mixing, represents a fundamental oceanographic question.

A seeming paradox has developed between indirect estimates of the turbulent eddy diffusivity (K) from advection-diffusion models and from budgeting studies (2, 3) and diffusivity estimates deduced from microstructure measurements (4). The mi-

crostructure-based estimates are typically an order of magnitude less than those inferred indirectly. However, few direct comparisons have been possible because the indirect schemes have been applied principally to the deep ocean, whereas most of the microstructure measurements have come from the upper 1 km of the ocean. One exception is the work of Moun and Osborn (5), who reported estimates of K derived from 11 velocity microstructure profiles to a maximum depth of 2240 m in the Northwest Pacific (three of which extended deeper than 1655 m). Their data suggested that eddy diffusivity increased with depth; extrapolation of Moun and Osborn's profile to abyssal depths yielded a diffusivity on the order of $1 \times 10^{-4} \text{ m}^2 \text{ s}^{-1}$, the canonical value obtained from vertical advective-diffusive models (2). We describe a somewhat larger set of 22 ocean microstructure (and fine-scale velocity) profiles extending to a depth of 3000 m (four of which are to 3800 to 4000 m).

From March to April of 1991 and 1992, vertical profiles of velocity and temperature microstructure were obtained with the free-

J. M. Toole and R. W. Schmitt, Woods Hole Oceanographic Institution, Woods Hole, MA 02543, USA. K. L. Polzin, School of Oceanography WB-10, University of Washington, Seattle, WA 98195, USA.

*To whom correspondence should be addressed.

fall High Resolution Profiler (HRP) (6) in the Northeast Pacific and Northeast Atlantic oceans, respectively. The eight profiles from the Pacific experiment that we examined were made 18 to 37 km from the summit of Fieberling Guyot (32.5°N, 127.7°W), a seamount that extends from depths between 4000 and 4500 m to within 500 m of the ocean surface. Of these eight, five were deemed representative of ocean interior conditions because fine-scale shear variance was within a factor of 2 of that due to the canonical internal wave field (7). The remaining three profiles were made over the deep flank of the seamount (water depth of approximately 3500 m) and exhibited elevated levels of fine-scale shear and microstructure at depths below 2000 m. We treated these three segments separately. Deep profiles were also obtained as part of the North Atlantic Tracer Release Experiment (NATRE) (8): 10 HRP deployments to 3000 m were made in a north-south transect along 26.7°W between 24° and 27.5°N in a water depth of approximately 5500 m. Supplementing these are a set of four profiles to depths of 3800 to 4000 m, one in the ocean interior (25.3°N, 23.3°W in 4900 m of water) and three over the African continental rise at 24.5°N, 20.3°W, where the bottom depth was 3900 m.

The intensity of velocity microstructure is reported in terms of the kinetic energy dissipation rate, ϵ ; we use the thermal dissipation rate, χ , to quantify the strength of the temperature microstructure (9). Noise levels are equated with the dissipation values at which ensemble-averaged spectra depart significantly from Nasmyth's (10, 11) empirical spectrum for velocity gradients and Batchelor's (12) theoretical spectra for temperature gradients. For the present measurements, the noise levels for ϵ and χ are approximately $1 \times 10^{-11} \text{ W kg}^{-1}$ and $1 \times 10^{-12} \text{ }^\circ\text{C}^2 \text{ s}^{-1}$, respectively. Error in the sensor calibrations and response functions, as well as the assumption of isotropy, leads to uncertainty in individual dissipation estimates. For values greater than the noise thresholds, we estimate that these measurement uncertainties (dominated by the isotropy assumption, which may bias the present results high) are no more than a factor of 2 about each value.

Turbulent eddy diffusivities (K_T , K_p) were derived by equating the production of turbulent variance to dissipation by molecular viscosity-diffusion. We used the Osborn and Cox (13) relation

$$K_T = \frac{\chi}{2} (\bar{\theta}_z)^{-2} \quad (1)$$

to obtain diffusivity values from averaged estimates of the intensity of temperature microstructure, and the Osborn (14) expression

$$K_p = \Gamma \epsilon N^{-2} \quad (2)$$

that relates the diffusivity to the averaged intensity of velocity microstructure through the mixing efficiency, Γ , taken here as constant: $\Gamma = 0.25$ (11). The mean vertical potential temperature gradient, $\bar{\theta}_z$, appears in Eq. 1, while in Eq. 2, N is the mean buoyancy frequency. The fundamental assumption behind these derivations is that production and dissipation do balance. This relation is thought to hold if the averaging procedures encompass many turbulent patches. The NATRE results (8) showing consistency between microstructure-based diffusivity estimates and those derived from dye dispersion gives credence to this assumption. Because individual dissipation estimates can vary over a wide range (4), it is also important that sufficient sampling is conducted to constrain the statistical uncertainty of the average values.

The ocean buoyancy profiles in the Northeast Pacific and Northeast Atlantic decreased roughly exponentially with depth below a vertical density gradient maximum at 100 to 200 m depth (Fig. 1). The associated buoyancy period increased from 20 min at 300 m to 2 hours at 3000 m. The ensemble-averaged dissipation rates from

the two ocean-interior sites decreased with depth on a scale comparable to that of the vertical density gradient (Fig. 2). There was indication at depth of somewhat larger average kinetic energy dissipation rates in the NATRE data and substantially greater mean temperature dissipation rates (Table 1). The larger χ values stemmed partly from more energetic turbulent eddies (larger ϵ values) that stirred the background vertical temperature profile and partly from the greater mean temperature stratification in the deep Northeast Atlantic.

The eddy diffusivity estimates that we derived from the mean dissipation values are small (about 0.1×10^{-4} to $0.5 \times 10^{-4} \text{ m}^2 \text{ s}^{-1}$) and approximately independent of depth within the statistical uncertainties (15) (Fig. 3). Diffusivities were somewhat greater at depth in the Northeast Atlantic than in the Northeast Pacific, but the averaged values from the two experiments (Table 1) were both smaller than those inferred from advective-diffusive models and budget calculations. The deep dissipation and eddy diffusivity estimates from the five Northeast Pacific interior profiles exhibited no spatial pattern, but the suggestion of a meridional gradient was found in the deep NATRE data. Individual profile-

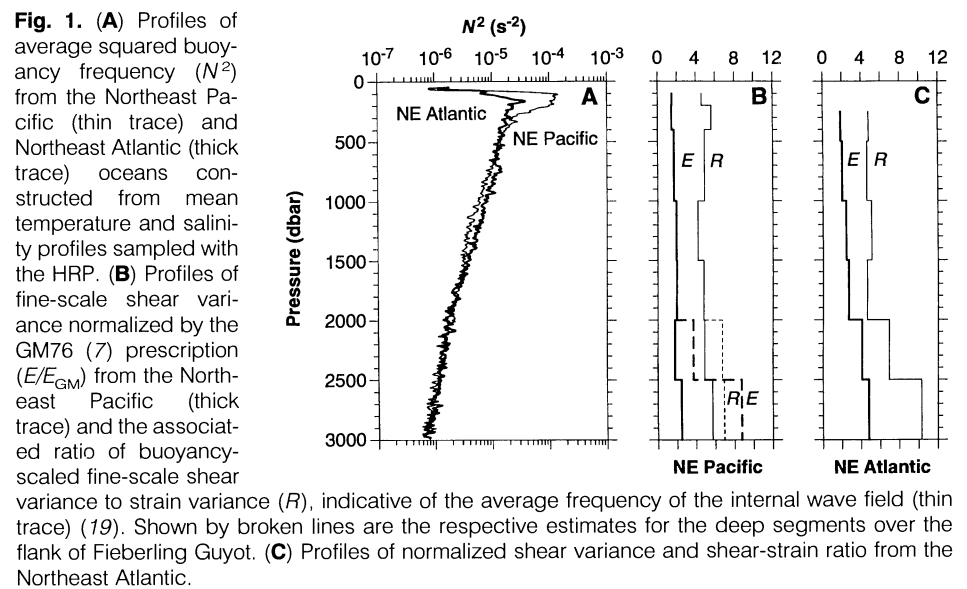


Table 1. Averaged dissipation rates and eddy diffusivity estimates from the three experiment sites for the interval 2500 to 3000 dbar with bootstrap uncertainty estimates. Errors appear in parentheses.

Location	Number of profiles	N (s^{-1})	ϵ ($10^{-10} \text{ W kg}^{-1}$)	χ ($10^{-10} \text{ }^\circ\text{C}^2 \text{ s}^{-1}$)	K_p ($10^{-4} \text{ m}^2 \text{ s}^{-1}$)	K_T ($10^{-4} \text{ m}^2 \text{ s}^{-1}$)
NE Atlantic	14	9.7×10^{-4}	1.02 (0.49)	0.94 (0.34)*	0.36 (0.20)	0.55 (0.22)*
NE Pacific						
Interior	5	9.3×10^{-4}	0.53 (0.08)	0.06 (0.002)	0.18 (0.04)	0.21 (0.08)
Near slope	3	9.3×10^{-4}	4.86 (1.51)	0.65 (0.16)	2.16 (0.65)	3.04 (1.04)

*Based on a subset of 10 profiles because of an instrumentation failure.

averaged K_p and K_T estimates for depths from 2000 to 3000 m increased from between 0.1×10^{-4} and $0.5 \times 10^{-4} \text{ m}^2 \text{ s}^{-1}$ south of 27°N to approximately $1 \times 10^{-4} \text{ m}^2 \text{ s}^{-1}$ at about 27.5°N .

Much more intense microstructure was observed in the deep segments of the three profiles over the flanks of Fieberling Guyot. The ensemble averaged dissipation values and the resulting eddy diffusivity estimates for the three guyot flank segments both increased with depth below 2000 m; the eddy diffusivities reached values of about $5 \times 10^{-4} \text{ m}^2 \text{ s}^{-1}$ at 3000 m (Figs. 2 and 3). These averaged quantities come from only three profiles, and it is not clear how representative they are of the typical conditions over the deep flank of the seamount. The trend of increasing eddy diffusivity as the bottom was approached was, however, a consistent feature of all the HRP profiles collected higher up the flank of Fieberling Guyot (a total of 80 profiles) (16). In contrast, the three HRP deployments in the Atlantic experiment above the African continental rise showed no increase on

approach to the bottom. The ensemble-averaged K_p value based on dissipation estimates below 3000 m was $0.11 \times 10^{-4} \pm 0.02 \times 10^{-4} \text{ m}^2 \text{ s}^{-1}$.

Enhanced mixing over the seamount flank as compared to that of the interior might have resulted from different internal wave characteristics. The dissipation rate ϵ has been related theoretically to the flux of energy through the internal wave field from large to small spatial scales (17, 18), which in turn is related to the diffusivity by Eq. 2. According to this theory, higher internal wave shear levels and higher average wave frequencies are associated with greater turbulent dissipation. The inferred internal wave shear in the far field of Fieberling Guyot is relatively constant with depth to 3000 m (Fig. 1B) at about twice the GM76 (7) intensity. The average wave field frequency inferred from the ratio of fine-scale shear and strain (19) is also independent of depth and close to that expected for the canonical wave field. In contrast, fine-scale shears over the deep flank of Fieberling Guyot increased with depth to approxi-

mately eight times the background value at 3000 m (Fig. 1B).

The bottom generation of waves, bottom reflection-scattering, or both might explain the perturbed internal wave fields in our observations. The kinematics of internal wave reflections from a sloping bottom can lead to the local enhancement of wave field energy density (20). In this linear theory, the affected wave frequencies are a function of the bottom slope; a steeper slope is associated with higher frequency for a given stratification. A modest increase in the shear to strain ratio (indicating lower-than-average wave field frequency) was observed above the deep flank of Fieberling Guyot as compared to the interior profiles (Fig. 1B). Consistent with simple ray-tracing arguments, this result suggests that we observed waves that had reflected off the bottom farther downslope where the bottom slopes are less than 0.1. The very small bottom slope of the African continental rise (0.006) could account for the lack of enhanced wave variance at that site (the bottom is effectively flat). Wave generation in a stratified fluid can arise from large-scale flow (the barotropic tide, for example) over bathymetric structures (21). Shear to strain ratios for the deep NATRE data (Fig. 2C) indicate the presence of very low frequency internal waves, perhaps indicative of strong internal tidal motions (22), near-inertial motions (23), or both, previously observed in the Northeast Atlantic. Theoretically (17, 18), the lower wave frequencies partially offset the tendency for higher dissipations due to the increased fine-scale shear level in these data (Fig. 1C), which results in the relatively constant profile of K_p .

The observations by Moum and Osborn in which K_p increased with depth may indicate that the internal wave shear level or average internal wave frequency increased with depth at their site. This trend with depth is the principal difference between our K_p profiles. Moum and Osborn's data were taken in the Kuroshio extension, where the deep internal wave field may have been influenced by strong flow over bathymetric features and interactions between the waves and the large-scale flow. The difference might also be caused by seasonality of the upper ocean internal wave field. Our data were collected in late winter, a time when the upper ocean internal wave energy is higher than that during early summer, when Moum and Osborn's measurements were made (24). Consistent with this idea, the upper ocean shear levels in our data were approximately twice the GM76 (7) value. Moum and Osborn did not observe the fine-scale velocity shear needed to quantify the characteristics of the internal wave field.

Our findings suggest that the abyssal

Fig. 2. Average kinetic energy dissipation profiles from the (A) Pacific and (B) Atlantic studies. Individual half-meter estimates of dissipation were depth-averaged in 200-m intervals and ensemble-averaged over the available profiles. Statistical uncertainties (shown shaded with diagonal lines) are given by a bootstrap technique (15). The deep curve segment in (A) derives from observations over the seamount flank.

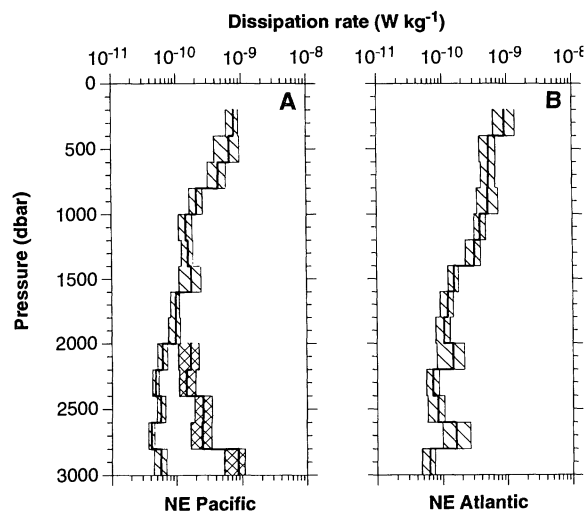
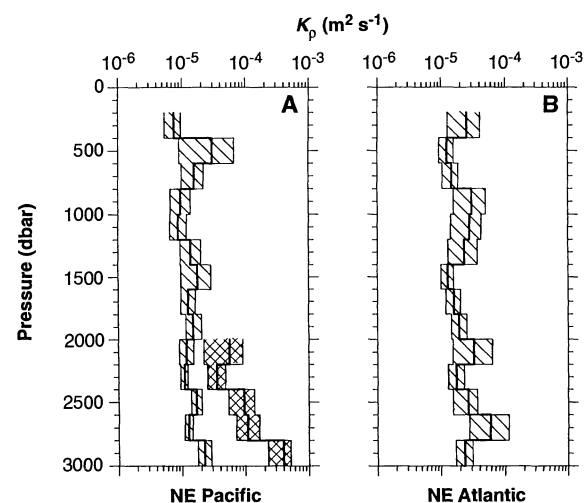


Fig. 3. Profiles of turbulent eddy diffusivity (K_p) from the (A) Pacific and (B) Atlantic studies derived from dissipation data and estimates of the mean buoyancy profiles. Statistical uncertainties (shown shaded with diagonal lines) are given by a bootstrap technique (15). The deep curve segment in (A) derives from observations over the seamount flank.



turbulent eddy diffusivity varies spatially and that the deviations are linked to variations of the internal wave field. The canonical internal wave field in the deep ocean interior appears to support only weak diapycnal mixing ($K_p \sim K_T \sim 0.1 \times 10^{-4} \text{ m}^2 \text{ s}^{-1}$). Large dissipation rates (supporting diffusivities much greater than $1 \times 10^{-4} \text{ m}^2 \text{ s}^{-1}$) seem possible in areas where the intensity of the internal wave field is enhanced. One such region is near the bottom where wave reflection, wave generation, or both can effectively perturb the background wave field. We believe the central question to be as follows: Can boundary processes alone account for the spatially averaged eddy diffusivity of $1 \times 10^{-4} \text{ m}^2 \text{ s}^{-1}$ or more that is derived by large-scale analyses (2)? Given an interior diffusivity of order $0.1 \times 10^{-4} \text{ m}^2 \text{ s}^{-1}$, hypsographic considerations (25) would seem to require large boundary diffusivities: perhaps 10×10^{-4} to $100 \times 10^{-4} \text{ m}^2 \text{ s}^{-1}$. Alternatively, bottom generation might cause the internal wave field to be generally enhanced at depth, which in turn would result in enhanced mixing. More extensive observations of microstructure and fine structure in the deep ocean and improved theories of internal wave generation and reflection at boundaries are needed.

REFERENCES AND NOTES

1. K. Wyrtki, *Deep-Sea Res.* **8**, 39 (1961).
2. W. H. Munk, *ibid.* **13**, 707 (1966).
3. N. G. Hogg, P. Biscaye, W. Gardner, W. J. Schmitz, *J. Mar. Res.* **40** (suppl.), 231 (1982).
4. A. E. Gargett, *ibid.* **42**, 359 (1984); M. C. Gregg, *J. Geophys. Res.* **92**, 5249 (1987); *J. Phys. Oceanogr.* **7**, 436 (1977).
5. J. N. Moum and T. R. Osborn, *J. Phys. Oceanogr.* **16**, 1250 (1986).
6. R. W. Schmitt *et al.*, *J. Atmos. Oceanic Technol.* **5**, 484 (1988).
7. The spectrum of the ocean internal wave field commonly exhibits universal characteristics, first described in mathematical form by C. Garrett and W. Munk [*Geophys. Fluid Dyn.* **3**, 225 (1972)]. This construct has been refined with time and the collection of additional data. We interpret our observations with reference to the spectrum presented by C. Garrett and W. Munk [*J. Geophys. Res.* **80**, 291 (1975)], as modified by J. L. Cairns and G. O. Williams [*ibid.* **81**, 1943 (1976)]. The shorthand notation for this description is GM76.
8. J. R. Ledwell, A. J. Watson, C. S. Law, *Nature* **364**, 701 (1993).
9. Turbulent scale velocity gradients were sampled with air-foil shear probes [T. R. Osborn, *J. Phys. Oceanogr.* **4**, 109 (1974)] calibrated at the Bedford Institute of Oceanography facility operated by N. Oakey. One-half-meter segments of velocity-gradient data were Fourier transformed and integrated to obtain estimates of shear variance. The integration was extended to a minimum in spectral energy density (beyond which the spectra were dominated by noise). The dissipation rates were derived on the assumption that the flow field was isotropic. Fast-response glass-bead thermistors (FP-07) were used to sample temperature microstructure; temperature gradient variance was also estimated in frequency space as outlined above, and the dissipation rate was derived on the assumption of isotropy. A thermistor calibration was constructed for each profile with

- data from a platinum resistance thermometer on the HRP, which in turn was calibrated in the Woods Hole Oceanographic Institution facility. Data from both microstructure sensors were corrected for probe and electronic interface responses before the estimation of the variance [K. L. Polzin, thesis, Woods Hole Oceanographic Institution/Massachusetts Institute of Technology Joint Program (1992)].
10. P. Nasmyth, thesis, Institute of Oceanography, University of British Columbia (1970).
 11. N. S. Oakey, *J. Phys. Oceanogr.* **12**, 256 (1982). Consistency of the K_T and K_p estimates reported in Table 1 suggest that $\Gamma = 0.25$ is, on average, a reasonable value. Taking a smaller value for Γ exacerbates the discrepancy between the indirect and microstructure-based estimates of the diapycnal diffusivity.
 12. G. K. Batchelor, *J. Fluid Mech.* **5**, 113 (1959).
 13. T. R. Osborn and C. S. Cox, *Geophys. Fluid Dyn.* **3**, 321 (1972).
 14. T. R. Osborn, *J. Phys. Oceanogr.* **10**, 83 (1980).
 15. The bootstrap method we used to derive uncertainty estimates followed the work of B. Efron and G. Gong [*Am. Stat.* **37**, 36 (1983)]. Dissipation profiles were depth-averaged over 10 m (yielding, according to run tests [M. C. Gregg, H. E. Sein, D. B. Percival, *J. Phys. Oceanogr.* **23**, 1777 (1993)], roughly independent samples) and binned into 200-m intervals. The binned populations were repeatedly subsampled and averaged. The error bars shown for each depth segment in Fig. 2 represent the 3rd and 97th percentile of the distribution of 100 mean estimates formed by the random sampling of one-half of the available data in each bin. These confidence intervals are not substantially different from the 95% confidence intervals based on an assumed log-normal distribution [M. A. Baker and C. H. Gibson, *ibid.* **17**, 1817 (1987)]. A similar procedure beginning with dissipation estimates normalized by vertical density and temperature gradients (computed over 20- to 50-m scales) yielded the error bars for diffusivity in Fig. 3 and Table 1. In consideration of the relatively small sample sizes, this error metric

may not represent the true uncertainty, particularly for the deep NATRE data that exhibited a meridional trend. The trend manifested itself as larger error bars for the average dissipation and diffusivity values for the Atlantic experiment than those for the Pacific.

16. J. M. Toole, E. Kunze, K. L. Polzin, R. W. Schmitt, *Eos* **75** (suppl.), 164 (1994).
17. F. S. Henyey, J. Wright, S. M. Flatte, *J. Geophys. Res.* **91**, 8487 (1986); F. S. Henyey, "Proceedings of 'Aha Huliko'a Hawaiian Winter Workshop," University of Hawaii at Manoa, 13 to 18 January 1991, *Sch. Ocean Earth Sci. Technol. Spec. Publ.* (1991), pp. 233–236; M. C. Gregg, *J. Geophys. Res.* **94**, 9686 (1989).
18. K. L. Polzin, J. M. Toole, R. W. Schmitt, unpublished data.
19. Linear wave theory provides a measure of average wave frequency from the ratio of buoyancy-scaled shear variance to strain variance [E. Kunze, A. J. Williams III, M. G. Briscoe, *J. Geophys. Res.* **95**, 18127 (1990)]. The terms in this ratio are estimated here by the respective integration of velocity and isopycnal displacement-gradient wave-number spectra to the fine-scale cutoff in the shear spectra (18).
20. O. M. Phillips, *The Dynamics of the Upper Ocean* (Cambridge Univ. Press, New York, ed. 2, 1977); C. C. Eriksen, *J. Geophys. Res.* **15**, 1145 (1985).
21. T. H. Bell, *J. Geophys. Res.* **80**, 320 (1975).
22. G. Siedler and U. Paul, *ibid.* **96**, 22259 (1991).
23. P. Saunders, *J. Phys. Oceanogr.* **13**, 1416 (1983).
24. M. G. Briscoe and R. A. Weller, *Dyn. Atmos. Oceans* **8**, 243 (1984).
25. L. Armi, *J. Geophys. Res.* **83**, 1971 (1978).
26. We thank the officers and crew of the R/V *New Horizon* and R/V *Oceanus*; E. Montgomery, R. Koehler, M. Cook, and D. Wellwood for technical support; and N. Oakey for advice and encouragement. Supported by the Office of Naval Research through grants (N00014-89-J-1073 and N00014-92-J-1323) to the Woods Hole Oceanographic Institution and by the National Science Foundation.

27 December 1993; accepted 31 March 1994

The Role of Mesoscale Tracer Transports in the Global Ocean Circulation

Gokhan Danabasoglu,* James C. McWilliams, Peter R. Gent

Ocean models routinely used in simulations of the Earth's climate do not resolve mesoscale eddies because of the immense computational cost. A new parameterization of the effects of these eddies has been implemented in a widely used model. A comparison of its solution with that of the conventional parameterization shows significant improvements in the global temperature distribution, the poleward and surface heat fluxes, and the locations of deep-water formation.

The oceans play important roles in regulating the Earth's climate and must be included when the effects of increasing greenhouse gases such as CO_2 are assessed. Sea-surface temperature largely dictates the heat flux between the atmosphere and ocean. The salinity of the upper ocean is also important in determining where deep-water formation occurs by convection. This deep-water formation drives the global

thermohaline circulation, sometimes called the ocean conveyor belt (1), which controls the horizontal transports of heat and fresh water and the absorption of increasing CO_2 in the atmosphere.

The most energetic oceanic motions occur on the mesoscale, with length scales of 10 to 100 km. The ubiquitous mesoscale eddies are important in the transports of heat, salt, and passive tracers such as radiocarbon and freon in all parts of the world's oceans. Their importance has been documented from observations in the Antarctic Circumpolar Current (ACC) (2) and the

National Center for Atmospheric Research, Boulder, CO 80307, USA.

*To whom correspondence should be addressed.